Rapid Coseismic Fault Determination of Consecutive Large Interplate Earthquakes: The 2011 Tohoku-Oki Sequence

Yusaku Ohta, Tatsuya Kobayashi, Ryota Hino, Tomotsugu Demachi, and Satoshi Miura

Abstract

Real-time monitoring of crustal deformation is important in achieving rapid understanding of earthquake magnitude and fault model. Recently, an algorithm called Real-time Automatic detection method for Permanent Displacement ("*RAPiD*") has been developed to detect/estimate static ground displacements due to earthquake faulting from real-time kinematic (RTK)-GPS time series. We applied this algorithm to the 2011 off Ibaraki earthquake (M_w 7.7), which occurred only 30 min after the 2011 Tohoku-Oki earthquake (M_w 9.0). The *RAPiD* algorithm worked well with the long baseline RTK-GPS time series for quasi real-time coseismic displacement detection and estimation. A quasi real-time fault determination was also attempted with an automatic detection/estimation displacement field. We found that the estimated moment release reached M_w 7.7 60 s after the origin time, almost the same as the actual seismic moment for this earthquake. We also assessed the long-term stability of the RTK-GPS time series under a 200-km baseline condition. We found the time series precision degraded slightly in summer compared with winter. However, the total stability is good for monitoring crustal deformation. These results suggest clearly that using real-time GPS data in conjunction with the *RAPiD* algorithm can provide rapid coseismic fault determination, even for consecutive large earthquakes.

Keywords

Rapid coseismic fault determination • RTK-GNSS (GPS) • The 2011 Tohoku earthquake • Tsunami early warning

1 Introduction

Real-time monitoring of crustal deformation is extremely important in achieving rapid understanding of earthquake magnitude and fault model. This is because the measured permanent displacement gives a direct indication of the true earthquake size (seismic moment magnitude, M_w), which in turn provides information for tsunami forecasting. Blewitt et al. (2006, 2009) proposed a potential key design for a Global Navigation Satellite System (GNSS)-based approach that could contribute to real-time earthquake source determination and tsunami warning. Sobolev et al. (2007) also proposed a near-field GPS array concept ("GPS-Shield") for the issuance of early tsunami warnings within 10 min after an earthquake. After these pioneering works, the 2011 off the Pacific coast of Tohoku earthquake (M_w 9.0) (hereafter, 2011 Tohoku earthquake) occurred, following which many efforts for rapid earthquake size determination based on real-time GNSS data have progressed. Melgar et al. (2012) proposed an algorithm (named "*fastCMT*") for the rapid determination of the moment tensor and centroid location for large earthquakes based on real-time high-rate GPS data. Wright et al. (2012) applied the precise point positioning strategy to the processing of GPS data for the 2011

Y. Ohta (✉) • T. Kobayashi • R. Hino • T. Demachi • S. Miura
Research Center for Prediction of Earthquakes and Volcanic Eruptions, Graduate School of Science, Tohoku University, Miyagi, Japan
e-mail: ohta@aob.gp.tohoku.ac.jp

C. Rizos, P. Willis (eds.), *IAG 150 Years*, International Association of Geodesy Symposia 143,
DOI 10.1007/1345_2015_109

Tohoku earthquake for rapid coseismic fault slip determination. Hoechner et al. (2013) applied the "GPS shield" concept proposed by Sobolev et al. (2007) to the 2011 Tohoku earthquake. They also estimated tsunami height along the coastline of Japan based on the estimated slip distribution on the plate interface. Their estimate was that the tsunami height exceeded 10 m around the central part of the Tohoku area. Colombelli et al. (2013) also developed an algorithm to invert for the slip distribution on the fault plane. Their "self-adapting" strategy does not require restrictive a priori assumptions about the ongoing earthquake. The initial fault plane used for the slip inversion is built based on quick preliminary magnitude estimation and the model is then upgraded as new values of the magnitude are established. Tsushima and Ohta (2014) reviewed near field tsunami forecasting based on the offshore tsunami data and onshore real-time GNSS data.

We also have developed an algorithm, called the Real-time Automatic detection method for Permanent Displacement (*RAPiD*), to detect/estimate static ground displacements due to earthquake faulting from real-time kinematic (RTK)-GPS time series (Ohta et al. 2012). The algorithm identifies permanent displacements by monitoring the difference between a short-term average (STA) and a long-term average (LTA) of the GPS time series, for which the characteristic function D is defined as follows:

$$D = |STA(t) - LTA(t)| - SD\,(LTA(t)) \tag{1}$$

where $LTA(t)$ and $STA(t)$ are the long- and short-term averages of the time series as functions of time t, respectively and $SD(LTA(t))$ represents the standard deviation of $LTA(t)$. $STA(t)$ and $LTA(t)$ are defined as follows:

$$STA(t) = \frac{\sum_{i=t-\alpha+1}^{t} p_i x_i}{\sum_{i=t-\alpha+1}^{t} p_i}, LTA(t) = \frac{\sum_{i=t-\beta+1}^{t} p_i x_i}{\sum_{i=t-\beta+1}^{t} p_i} \tag{2}$$

where x_i is the norm of the horizontal components at $t = i$. And, α and β are the proper time-window lengths. In the work by Ohta et al. (2012), they used 60 and 600 s for the values of α and β, respectively. This selection of time-window length is based mainly on the source time length of the tsunamigenic earthquake. The p_i is a weighting parameter based on the quality of the RTK-GPS time series. For the detection of the displacement, Ohta et al. (2012) define a threshold value K before the monitoring. When $D > K$, the occurrence of displacement is recognized. Please refer to Ohta et al. (2012) for more detailed information on the *RAPiD* algorithm. Ohta et al. (2012) applied the algorithm to data pertaining to the 2011 Tohoku earthquake (M_w 9.0) to test the possibility of coseismic displacement detection based on the GNSS Earth Observation Network System (GEONET) 1-Hz data. Furthermore, the obtained displacement fields were inverted for a fault model. The inversion estimated a fault model with Mw 8.7, which is close to the actual M_w value of 9.0, within 5 min from the origin time (Ohta et al. 2012).

The 2011 Tohoku earthquake not only caused the mainshock, but also large aftershocks. One of the large aftershocks occurred only 30 min after the mainshock; this was the earthquake off Ibaraki, which was an interplate earthquake with magnitude M_w 7.7 (estimated by the JMA). Monitoring consecutive large earthquakes such as these is important for the prevention of secondary damage caused by tsunamis. For the M_w 7.7 aftershock in the off Ibaraki case, the earthquake early warning system (EEW) of the JMA did not work because of high background noise from the coda waves of the mainshock and other active aftershocks, and because of power failures and wiring disconnections (Hoshiba et al. 2011). Over the past 1,000 years, large earthquakes (around M_w 8.0) have occurred repeatedly every 100–200 years along the Nankai Trough in southwestern Japan, where the Philippine Sea plate is being subducted beneath the Amurian plate. The most recent large events were the 1944 Tonankai earthquake and the 1946 Nankai earthquake and furthermore, we expect the next large interplate earthquakes to occur along the Nankai Trough. Some past events have occurred consecutively, for example, the 1854 Ansei earthquake first ruptured the Tonankai and Tokai segment, and then 32 h later the Nankai segment was ruptured. Based on these past cases of huge interplate earthquakes, a robust earthquake and tsunami early warning system based on various seismic and geodetic sensors is required. In this short report, we perform an a posteriori analysis of the 2011 off Ibraki earthquake, which was one of the large aftershocks of the 2011 Tohoku earthquake, to test our quasi real-time approach to crustal displacement detection/estimation. We also discuss briefly the long-term stability of the RTK-GPS time series based on Japan's nationwide GEONET data.

2 Data and Analysis

2.1 RTK-GPS Analysis and Its Assessment for Long-Term Precision Stability

We used GEONET data for this short report. For the RTK-GPS analysis, we used RTKLIB v. 2.4.1. (RTKLIB; an open source program for GNSS positioning, http://www.rtklib.com), which features the long baseline RTK-GNSS technique for detecting deformation caused by earthquakes

for baselines over several hundreds of kilometers. In this analysis, we only used the GPS satellite system for the monitoring large-scale crustal deformation.

The precision of the RTK-GPS time series depends strongly on the baseline length. Thus, Ohta et al. (2012) showed that the baseline-length-dependent precisions of RTK-GPS time series, if ultra-rapid orbit information from the International GNSS Service (IGS) (Dow et al. 2009) is used, are within the ranges of 1.2–3.3 mm/100 km and 3.3–8.6 mm/100 km of standard deviation for the horizontal and vertical components, respectively. These results indicate that the precisions of baseline estimation are 12–33 mm for the horizontal and 33–86 mm for the vertical components, respectively, for a baseline length of 1,000 km. It was suggested that this is sufficiently precise for fault model estimation of large earthquakes, because 1,000 km is a sufficient distance, given that the base station for the RTK-GPS is set at this distance from the epicenter to avoid coseismic steps, even for huge earthquakes. For monitoring purposes, long-term stability, such as monthly to yearly, is also an important factor because false alarms must be avoided for a reliable warning system. Thus, we also assess the long-term stability of the RTK-GPS time series.

For the assessment of the long-term stability of RTK-GPS time series, we chose sites 0036 and 0585 as the reference and rover sites, respectively (Fig. 1), for which the baseline length is 200 km. For real-time orbit information, we used the ultra-rapid orbit products provided by the IGS and broadcast orbit information (e.g., Boyd 2009). The precise orbit information provides us exact GPS satellite positions relative to the WGS-84 reference frame. The precise ephemeris consists of two parts: an observed part and predicted part (predicted part of IGS ultra-rapid orbit, hence IGUP), which is estimated by extrapolation from past GPS satellite positions and can be obtained in real time. In contrast, the broadcast orbit (hereafter BRDC) is transmitted directly from GPS satellites to receivers using the Keplerian factors format. We processed the 30-second-interval raw data for the entire year of 2009 based on the BRDC and IGUP orbit information, and Fig. 2 shows the results. The calculated standard deviations (SDs) of the entire yearly time series are also summarized in Fig. 2. It is clear that the calculated SDs with IGUP are less than 20 and 50 mm in the horizontal and vertical components, respectively, and even for the BRDC result, the SDs are less than 30 and 60 mm in each component. In Fig. 2, a diagonal pattern in the time series can be seen clearly. This is caused by multipath errors, which are highly repeatable from day to day with a sidereal period (23 h 56 m 4 s) (e.g., Bock 1991; Choi et al. 2004; Larson et al. 2007). Choi et al. (2004) suggested that "orbit repeat filtering" (repeating time: 23 h 55 m 55 s) is better than pure sidereal filtering. In Fig. 2, we also found that the precision of the time series degrades in summer compared with winter. The degradation in summer may be caused by difficulties involving time-dependent tropospheric effects and estimations of its component's gradients. Interestingly, the SDs in the horizontal components are less than 30 mm, even through the summer. This suggests that the RTK-GPS time series is largely stable throughout the year, despite the small annual pattern detected. Based on this example, we conclude that the RTK-GPS time series is stable enough for the monitoring of large-scale crustal deformation.

2.2 A Posteriori Analysis of the 2011 Off Ibaraki Earthquake

For the a posteriori processing of the 2011 off Ibaraki earthquake, we used station 0065 as the reference site (Fig. 1). For the assessment of the detection of the occurrence of consecutive earthquakes by our *RAPiD* algorithm, we used GPS data from the occurrence of the M9 Tohoku earthquake until the end of the off Ibaraki earthquake. The other detailed settings of the RTK-GPS processing strategies are the same as those detailed in Ohta et al. (2012). To simplify crustal deformation monitoring, we did not apply sidereal filtering to the RTK-GPS time series in this study.

3 Application to the Aftershock of the 2011 Tohoku Earthquake

3.1 Example of Displacement Detection/Estimation Process

Figure 3 shows an example of the time series of the RTK-GPS data and the characteristic function D values (see Eq. 1) defined by the *RAPiD* algorithm at GEONET station 3009 on March 11, 2011, when the M_w 9.0 Tohoku earthquake and its aftershock occurred. Owing to the coseismic displacement of the mainshock, the D value based on the horizontal components started increasing and exceeded the threshold level (red line) for event detection. Figure 3 also shows the off Ibaraki earthquake as the M9 aftershock. For this station, the coseismic displacement of this aftershock is clearly larger than that of the mainshock. Figure 3 indicates clearly that the *RAPiD* algorithm works under the circumstance of consecutive earthquake occurrence. On the other hand, the D value based on the horizontal components clearly shows a negative value after the M9 mainshock (Fig. 3). For the *RAPiD* algorithm, the $SD(LTA(t))$ is introduced to avoid false alarms caused by strong ground shaking. This means avoiding false alarms when there is no permanent displacement with strong ground shaking; thus, the $SD(LTA(t))$ must be large after the mainshock. The result found was that the value of D decreased within the window length of the LTA. Therefore,

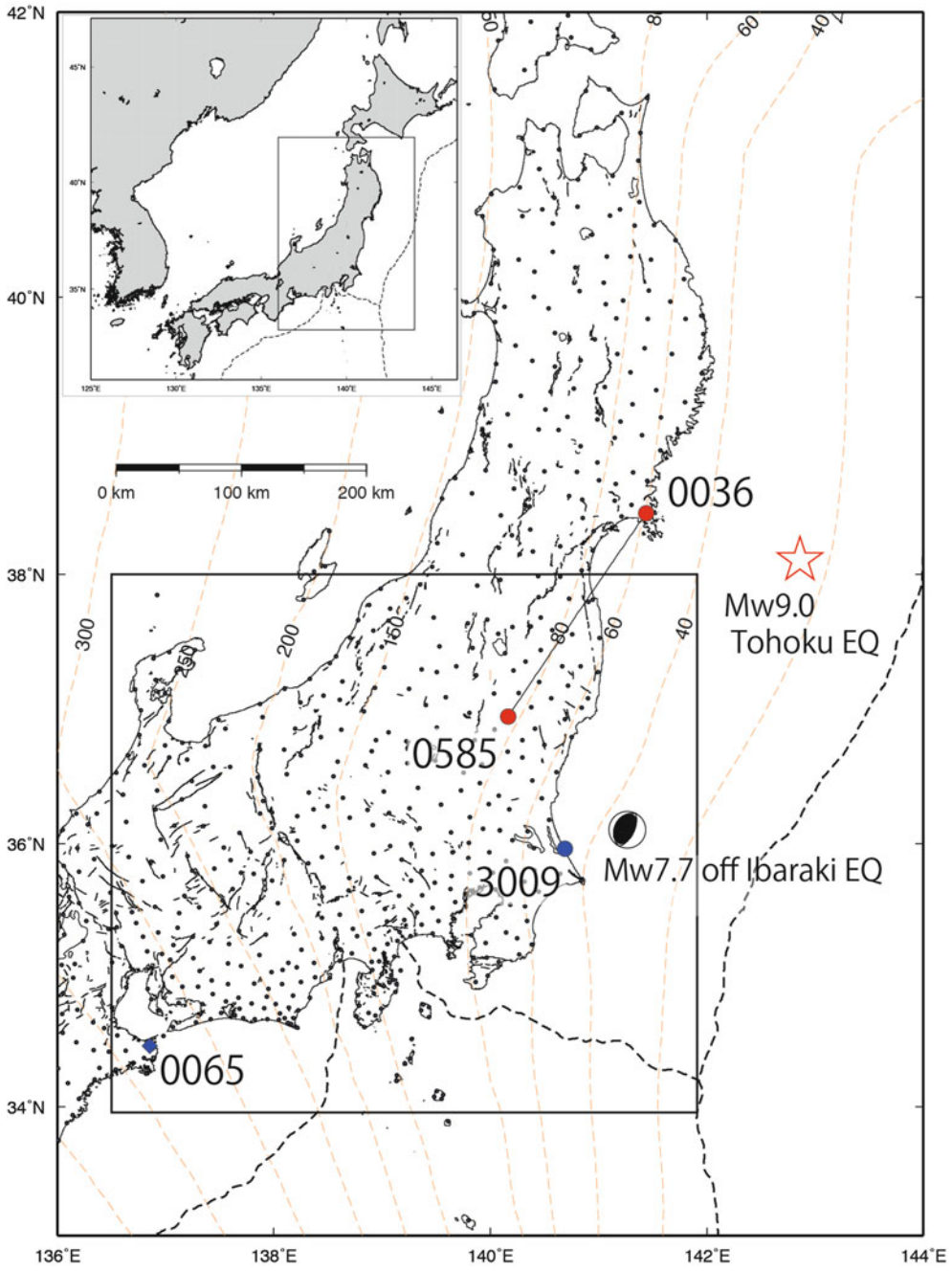

Fig. 1 GPS site distribution for this study. *Black circles* denote GEONET sites. The *red circles* denote the GEONET stations for the assessment of long-term stability in Sect. 2.1. The *blue diamond* denote the reference station for the posteriori processing for the M_w 9.0 Tohoku earthquake and its aftershock. The blue circle denote the location of example station for figure 3. The *black rectangular region* denotes the study area for the a posteriori coseismic fault determination for the 2011 off Ibaraki earthquake. The *open red star* represents the hypocenter of the 2011 Tohoku earthquake determined by the JMA. The mechanism solution represents the 2011 off Ibaraki earthquake determined by the National Research Institution for Earth Science and Disaster Prevention. The *orange dashed contours* denote the subducting Pacific plate compiled by Nakajima and Hasegawa (2006)

the permanent displacement detection ability of the *RAPiD* algorithm will decrease just after the large earthquake. The length of this low performance window is strongly dependent on the LTA window length and duration of ground shaking during the preceding earthquake. In the example case, the low performance time is around 10 min after the mainshock, which is almost the same as with the LTA window length (600 s). We believe this short time period (∼10 min) is an acceptable range for the detection of consecutive large earthquakes. One idea for avoiding the low performance time

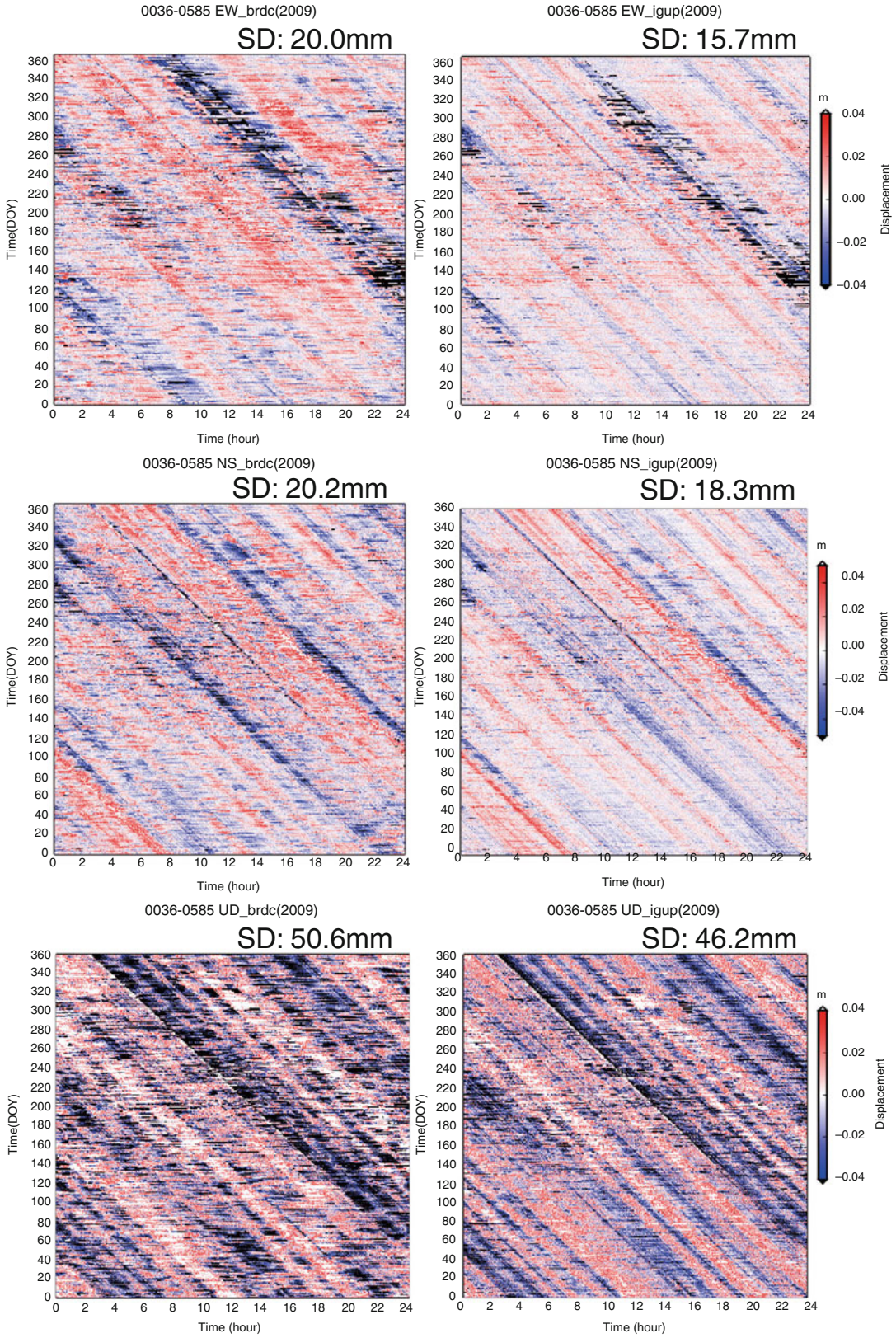

Fig. 2 Three-component RTK-GPS time series during DOY1-365, 2009 at station 0585 referred to station 0036 using broadcast orbit (left row, EW, NS, and UD) and IGS ultra-rapid orbit information (right row, EW, NS, and UD). The *vertical axis denotes* the DOY in 2009 and the *horizontal axis* denotes the hours in the day. The *color* indicates the perturbation of the coordinates from the averaged daily position: *red color* positive perturbation and *blue color* negative perturbation. The SD of the time series is presented in each figure

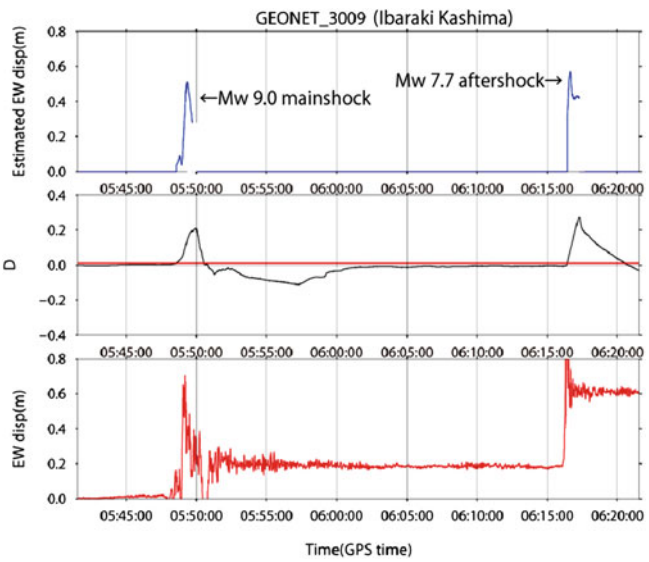

Fig. 3 Time series example of the 2011 Tohoku earthquake and its aftershock at GEONET site 3009 referred to the station 0065. *Top*, *middle*, and *bottom row* represent the norm of the horizontal component time series, the *D* value, and the raw EW component time series, respectively. The *red line* in the middle time series represents the threshold value *K*, determined previously based on each baseline's noise level

just after the large event is a flexible LTA value. In the *RAPiD* algorithm, the event detection restarts when the *D* value is lower than the threshold value *K*. If we make the LTA time-window length shorter than the original in this timing for the consecutive large events, then the low performance time will also become shorter. It is to be noted that even though the low performance time window exists, the *RAPiD* algorithm might still detect sufficiently large coseismic displacements.

Next, we show quasi real-time fault determination based on the *RAPiD* algorithm for this aftershock.

3.2 Quasi Real-Time Fault Determination for the 2011 Off Ibaraki Earthquake

Figure 4 shows several snapshots of the three-component coseismic displacement fields based on the *RAPiD* algorithm. It is clear that the large displacement is evident mainly in the horizontal component. We also estimated the coseismic fault plane based on the estimated permanent displacement. The estimated coseismic displacement fields were inverted repeatedly for a rectangular fault model at a time interval of 15 s using a nonlinear inversion method with a priori information (Matsu'ura and Hasegawa 1987). In the inversion, Green's function was used, which relates fault motion to surface displacement in an elastic half-space (Okada 1992). The estimated parameters occasionally depend on the initial values assumed in the recursive procedure. To estimate all the fault parameters (location, depth, length, width, strike, dip, rake, and slip amount), we assumed initial values for the fault location. We used the first coseismic displacement detection GPS site information for the initial fault location. In this analysis, *RAPiD* algorithm detected coseismic displacement 35 s after the origin time in station 3022 (Fig. 4). We used the coordinate of this station for initial fault location. When the initial horizontal fault location determined, the initial fault depth could also determine based on the model of the subducting plate interface (e.g. Nakajima and Hasegawa 2006). We also assumed the fault length, width, and slip amount with very large uncertainty. We gave uncertainty for these initial fault parameters for the inversion analysis: fault location (3.5° in latitude and longitude), depth (20 km), fault length (50 km), width (50 km), and slip amount (7 m). We gave the relatively strong constraint to the other parameters (strike, dip and rake angle) with interplate earthquake into consideration. For the actual operation, the EEW by JMA based on the seismic data will be useful for the determination of initial fault parameters. Even if the EEW does not work, we can assume the initial fault location based on the coseismic displacement information by GPS data.

The estimated simple rectangular fault model explains the displacement data basically well (Fig. 4). The temporal change in the coseismic fault shows the rupture expansion. At 45 s after the earthquake, the estimated coseismic fault model did not explain the coseismic displacement field. It may be caused by the ongoing rupture process along the fault plane. At 60 s after the earthquake, the estimated moment magnitude had already reached M_w 7.7 (assumed rigidity: 40GPa). At this point, the coseismic fault rupture was almost complete, based on the GPS displacement fields. Furthermore, 180 s after the earthquake, all of the GPS sites completed the displacement estimations, and we assigned this length of time to the final coseismic fault model for this earthquake. The estimated moment magnitude finally reached M_w 7.7, which slightly smaller than the seismological results. The Global CMT (centroid moment tensor) Project estimated a value of M_w 7.9 from the CMT inversion for this earthquake. Kubo et al. (2013) also estimated the coseismic slip distribution based on the strong-motion and post-processing

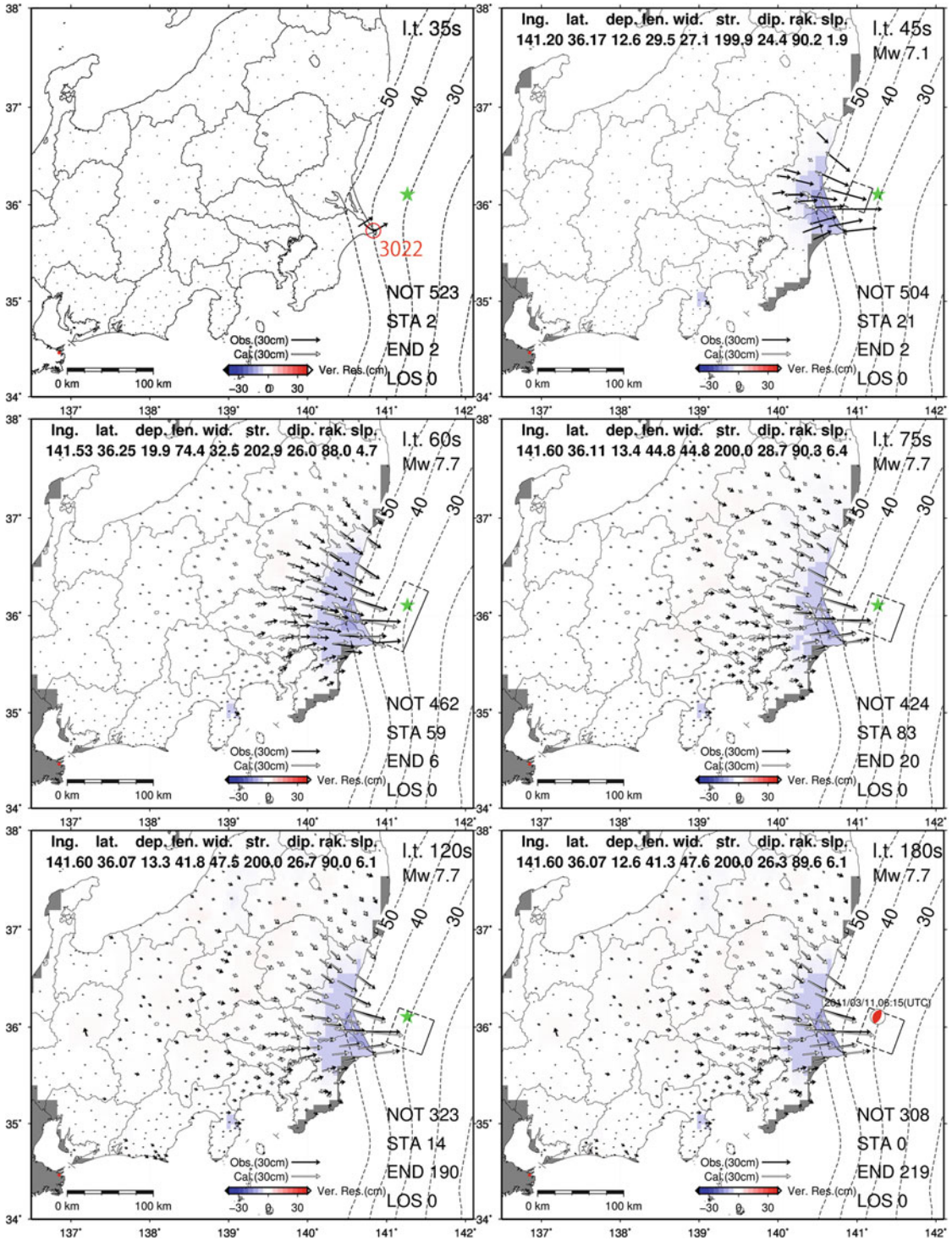

Fig. 4 Several snapshots at 15-second intervals of the three-component GPS displacement and automatically estimated fault model for the 2011 off Ibaraki earthquake using the data up to the lapse time (l.t. measured from the origin – shown in the *upper right* of each respective snapshot). Snapshot of 35 s after the earthquake is consistent with the first coseismic displacement detection timing in the GEONET 3022 site (*red circle*). *Black rectangular areas* denote the fault model estimated at each lapse time. Details of the estimated fault model parameters are shown above each snapshot. Longitude, latitude, and depth denote the location of the upper-left corner of rectangular fault plane, looking down from the hanging wall side. *Black vectors* represent observed horizontal displacements. The *open vectors* indicate calculated horizontal displacements based on the estimated fault model. The *colors* indicate residual between observed and calculated (O–C) value of the vertical component. NOT, STA, END, and LOS in the lower right of each snapshot represent the numbers of stations judged before signal arrival, during displacement increase, after final displacement, and troubled, respectively. The mechanism solution in 180 s after the origin time represents the F-net solution for the 2011 off Ibaraki earthquake determined by NIED

kinematic GPS analysis. Their results showed the estimated moment magnitude and the maximum slip were M_w 7.9 and 6.3 m, respectively. This underestimation might be mainly caused by errors in the estimation of the fault depth during our inversion.

The estimated coseismic fault model was located clearly (around 10–15 km) shallower than the actual subducting plate interface (Fig. 4). For the inversion, we considered an interplate earthquake by the initial fault parameter assumption. The estimated fault parameters, however, have strong trade off between each other. For example, the fault depth and slip amount on the fault had large correlation. Thus, our estimated fault plane was not forced to be on the subducting plate interface.

For the actual monitoring, we should pay attention not only interplate earthquake, but also other types of the earthquake mechanism. In fact, the large intraslab earthquake (M7.1) occurred in April 7 2011 at the Miyagi-Oki region, which is located within the rupture area of the 2011 Tohoku earthquake (e.g. Ohta et al. 2011). For such case, the initial fault parameters are very important for the rapid fault model estimation. As described in the Introduction, Melgar et al. (2012) developed "*fastCMT*" algorithm for the rapid determination of the moment tensor and centroid location. Such approach may be important for the initial focal mechanism determination.

An M7–8 class earthquake is expected to exhibit a source-time function duration of several tens of seconds to a few minutes. Our *RAPiD* algorithm can define the "final" solution (180 s) based on the number of GPS sites with completed displacement. On the other hand, after 60 s from the onset of the earthquake, our estimation result (M_w 7.7) had already reached agreement with the actual one (M_w 7.9 by GCMT solution). This suggests that the use of our algorithm would make it possible to raise an alert before the "final" solution, which would be useful for a timelier earthquake and/or tsunami early warning system. Furthermore, the source time function is not only a factor for effective tsunami excitation, but also for the rupture velocity and its expansion. Thus, the real-time onshore GPS data are useful not only for estimation of the magnitude, but also for the fault expansion and time dependence of the fault rupture. Of course, the estimated point source deduced from seismological/geodetical data can be translated to the finite fault model experimentally by applying the scaling law between fault dimension and magnitude. In the case of large earthquakes, however, the relationships between coseismic fault expansion and its aspect ratio are diverse. This is because the width and length of the seismogenic zone differ between each subduction zone. Based on the above, it can be stated that onshore GPS data have an advantage in the robust estimation of coseismic fault dimension, location, and its slip amount.

4 Conclusion

We applied the *RAPiD* algorithm to the 2011 off Ibaraki earthquake, which was one of the large aftershocks following the 2011 Tohoku earthquake. The *RAPiD* algorithm worked well with the long baseline RTK-GPS time series for quasi real-time coseismic displacement detection/estimation. A quasi real-time fault determination was also attempted with an automatic detection/estimation displacement field. We found that the estimated moment release 60 s after the origin time reached M_w 7.7, which was almost similar to the actual moment magnitude for this earthquake. Furthermore, we established the length of the low performance time window of the *RAPiD* algorithm just after the large earthquake. For the 2011 Tohoku sequence, the low performance time was around 10 min after the mainshock. This period might be an acceptable length for the detection of consecutive large earthquakes. We also assessed the stability of the RTK-GPS time series for the entire year and found that it demonstrated a highly repeatable day-to-day pattern with a sidereal period caused by the multipath effect. We found that the time series disturbance in summer was slightly larger than in winter. Based on this analysis, it is concluded that the RTK-GPS time series is basically stable enough for the monitoring of crustal deformation. These results suggest that the RTK-GPS data and our algorithm are useful for rapid coseismic fault determination, even for consecutive large earthquakes.

Acknowledgements The authors would like to thank Prof. Manabu Hashimoto and Prof. Jeffrey T. Freymueller for their invitation to the International Association of Geodesy Scientific Assembly in Potsdam. The paper benefited from careful reviews by Dr. Ronni Grapenthin, Prof. Jeffrey T. Freymueller and two anonymous reviewers. We thank the GSI for providing GPS data. We are also very grateful to IGS for providing high-quality precise ephemerides as well as real-time observation data from their tracking stations. This study was supported partly by a grant-in-aid for young scientists (start-up 19840006) from the Research of Japan Society for the Promotion of Science. This study was also supported by the project of the Ministry of Education, Culture, Sports, Science and Technology, Japan, titled "Observation and Research Program for the Prediction of Earthquakes".

References

Blewitt G, Kreemer C, Hammond WC, Plag H-P, Stein S, Okal E (2006) Rapid determination of earthquake magnitude using GPS for tsunami warning systems. Geophys Res Lett 33:L11309. doi:10.1029/2006GL026145

Blewitt G, Hammond WC, Kreemer C, Plag H-P, Stein S, Okal E (2009) GPS for real-time earthquake source determination and tsunami warning systems. J Geod 83:335–343. doi:10.1007/s00190-008-0262-5

Bock Y (1991) Continuous monitoring of crustal deformation. GPS World 2(6):40–47

Boyd D (2009) GPS constellation status and performance. Paper presented at 49th Meeting, Civ. GPS Serv. Interface Comm., Savannah, Ga

Choi K, Bilich A, Larson K, Axelrad P (2004) Modified sidereal filtering: implications for high-rate GPS positioning. Geophys Res Lett 31:L22608. doi:10.1029/2004GL021621

Colombelli S, Allen RM, Zollo A (2013) Application of real-time GPS to earthquake early warning in subduction and strike-slip environments. J Geophys Res 118(7):3448–3461. doi:10.1002/jgrb.50242

Dow JM, Neilan RE, Rizos C (2009) The international GNSS service in a changing landscape of global navigation satellite systems. J Geod 83:191–198. doi:10.1007/s00190-008-0300-3

Hoechner A, Ge M, Babeyko AY, Sobolev SV (2013) Instant tsunami early warning based on real-time GPS - Tohoku 2011 case study. Nat Hazards Earth Syst Sci 13(5):1285–1292. doi:10.5194/nhess-13-1285-2013

Hoshiba M, Iwakiri K, Hayashimoto N, Shimoyama T (2011) Outline of the 2011 off the pacific coast of Tohoku earthquake (Mw 9.0)—earthquake early warning and observed seismic intensity. Earth Planets Space 63(7):547–551. doi:10.5047/eps.2011.05.031

Kubo H, Asano K, Iwata T (2013) Source-rupture process of the 2011 Ibaraki-oki, Japan, earthquake (M w 7.9) estimated from the joint inversion of strong-motion and GPS Data: relationship with seamount and Philippine Sea Plate. Geophys Res Lett 40(12):3003–3007. doi:10.1002/grl.50558

Larson KM, Bilich A, Axelrad P (2007) Improving the precision of high-rate GPS. J Geophys Res 112:B05422. doi:10.1029/2006JB004367

Matsu'ura M, Hasegawa Y (1987) A maximum likelihood approach to nonlinear inversion under constraints. Phys Earth Planet Int 47:179–187. doi:10.1016/0031-9201(87)90076-8

Melgar D, Bock Y, Crowell BW (2012) Real-time centroid moment tensor determination for large earthquakes from local and regional displacement records. Geophys J Int 188:703–718. doi:10.1111/j.1365-246X.2011.05297.x

Nakajima J, Hasegawa A (2006) Anomalous low-velocity zone and linear alignment of seismicity along it in the subducted Pacific slab beneath Kanto, Japan: reactivation of subducted fracture zone? Geophys Res Lett 33:L16309. doi:10.1029/2006GL026773

Ohta Y, Miura S, Ohzono M, Kita S, Iinuma T, Demachi T, Tachibana K, Nakayama T, Hirahara S, Suzuki S, Sato T, Uchida N, Hasegawa A, Umino N (2011) Large intraslab earthquake (2011) after the 2011 off the Pacific coast of Tohoku earthquake (M9.0): coseismic fault model based on the dense GPS network data. Earth Planets Space 63(12):1207–1211. doi:10.5047/eps.2011.07.016

Ohta Y, Kobayashi T, Tsushima H, Miura S, Hino R, Takasu T, Fujimoto H, Iinuma T, Tachibana K, Demachi T, Sato T, Ohzono M, Umino N (2012) Quasi real-time fault model estimation for near-field tsunami forecasting based on RTK-GPS analysis: application to the 2011 Tohoku-Oki Earthquake (Mw 9.0). J Geophys Res 117:B0231116. doi:10.1029/2011JB008750

Okada Y (1992) Internal deformation due to shear and tensile faults in a half-space. Bull Seismol Soc Am 82:1018–1040

Sobolev SV, Babeyko AY, Wang R, Hoechner A, Galas R, Rothacher M, Sein DV, Schröter J, Lauterjung J, Subarya C (2007) Tsunami early warning using GPS-Shield arrays. J Geophys Res 112(B8):1–18. doi:10.1029/2006JB004640

Tsushima H, Ohta Y (2014) Review on near-field tsunami forecasting from offshore tsunami data and onshore GNSS data for tsunami early warning. J Disaster Res 9(3):339–357

Wright TJ, Houlié N, Hildyard M, Iwabuchi T (2012) Real-time, reliable magnitudes for large earthquakes from 1 Hz GPS precise point positioning: the 2011 Tohoku-Oki (Japan) earthquake. Geophys Res Lett 39:1–5. doi:10.1029/2012GL051894